View Article Online / Journal Homepage / Table of Contents for this issue
Dynamic Article Links

Nanoscale

Cite this: *Nanoscale*, 2012, **4**, 7664

www.rsc.org/nanoscale

PAPER

Plasmonic coupled nanotorch structures leading to uniform surface enhanced Raman scattering detection

Haiping M. Chen,*[a] Lin Pang,[a] Andrew King,[b] Grace M. Hwang[c] and Yeshaiahu Fainman[a]

Received 16th August 2012, Accepted 11th September 2012
DOI: 10.1039/c2nr32305b

Published on 14 September 2012 on http://pubs.rsc.org | doi:10.1039/C2NR32305B
Downloaded by University of California - San Diego on 03 December 2012

Nanocrescent-like structures have become important surface enhanced Raman scattering structures because instead of relying on a few nanometer gap inter-particle plasmonic coupling to achieve local field enhancement, intra-particle plasmonic coupling between the cavity modes and the tip edges are utilized to achieve high local field enhancement at the tips. Our fabrication approach creates 'nanotorch' structures with controllable cavity rim opening and deterministic orientation to yield uniform Raman measurements, consisting of three-dimensional upright-oriented nanocrescent structures resting on nanopillars. Each structure serves as a single SERS substrate. We demonstrate that a nanotorch with a smaller rim opening results in a higher enhancement factor compare to one with a larger opening. More importantly, the uniformity of all the analysed Raman modes of adsorbed benzenethiol is better than 80% due to the consistent, upright orientation of each single nanotorch SERS substrate, paving the way for practical implementation of SERS detection.

1. Introduction

Surface enhanced Raman scattering (SERS) detection has gradually become a powerful tool from material identification to single molecule detection. However, fabrication of new SERS substrates is still heavily investigated due to two unsolved issues: achieving high local field enhancement (LFE) while simultaneously giving high repeatability. Solving this will be crucial for commercialization of SERS substrates. Nanoparticles were first used as SERS substrates, but were soon replaced by nanoparticle assemblies offering higher LFE at the interstitial sites due to coupling between particles. However, the random locations of the hot spots made the substrate impossible for quantitative analysis of the reagents. Other approaches were pursued; electron beam lithography and focused ion beam were employed to fabricate finely defined nanostructures, such as bowtie structures for high LFE at the tips,[1] but high cost and the planar methodology would prohibit successful commercialization. Subsequently, researchers have studied multiple resonances coupling of nanocrescent or half-shell structures[2–9] (where coupling among tip-to-tip, tip-to-cavity, cavity-to-body are involved), of the ring and disc structure[10] (where coupled multiple dipoles are involved), and of the composite nanocrescent and disc structure[11] (where dipole to quadruple coupling are involved). Nanocrescents have become useful SERS structures because they are one of the most structurally and optically tunable anisotropic metal nanostructures. Unlike structures that rely on a few nanometer gap inter-particle plasmonic coupling to achieve high LFE, the nanocrescents are fabricated from relatively large sacrificial nanoparticles with diameters of a few hundred nanometers. The nanoparticle size can be used to tune the plasmonic resonance.

It was shown in two-dimensional (2-D) nanocrescents that decreasing the tip distance will localize the field to a smaller volume and therefore increase the value of its complex amplitude.[3,5] However, such field localization and enhancement have not been demonstrated experimentally for three-dimensional (3-D) nanostructure to fully realize the different types of coupling, especially the tip-to-tip coupling of a small gap. Most importantly, the orientation control of 3-D nanocrescents that is required for high SERS repeatability has not been demonstrated, especially when used as a single SERS substrate.

Here, we demonstrate a new variant of the nanocrescent, the 'nanotorch' structure, yielding smaller tip-to-tip spacing (in 3-D, smaller rim diameter) with higher LFE. Furthermore, unlike previous 3-D nanocrescent fabrication methods that yielded randomly oriented nanocrescent structures, we demonstrate a fabrication method where the nanotorches are upright on their carrier substrate with controllable rim diameter and deterministic orientation. These nanotorch structures are beneficial for biosensing application, because they induce the maximum LFE for normal photon incidence and yield repeatable Raman measurements with less than 20% standard deviation. This will not only improve the limit of detection, but also increase the spatial resolution of SERS detection when the nanotorches are arranged in a periodic array, greatly impacting applications ranging from single molecule detection to *in vivo* diagnosis.

[a]*Department of Electrical and Computer Engineering, University of California, San Diego, La Jolla, CA 92093-0407, USA. E-mail: fainman@ece.ucsd.edu*
[b]*Renishaw Inc., 5277 Trillium Blvd., Hoffman Estates, Il 601923, USA*
[c]*The MITRE Corporation, 2275 Rolling Run Drive, Woodlawn, MD 21244, USA*

This journal is © The Royal Society of Chemistry 2012

Published on 14 September 2012 on http://pubs.rsc.org | doi:10.1039/C2NR32305B
Downloaded by University of California - San Diego on 03 December 2012

2. Results and discussions

2.1 Finite element method simulation

We investigated the nanotorch structure with full 3-D finite element method (FEM) simulations. The nanotorch is composed of a nanocrescent structure on top of a pillar with a refractive index of 1.47. A planar nanocrescent model was first formed by subtracting an inner circle with a 150 nm radius, offset from the center by 50.5 nm, from an outer circle with a 200 nm radius, yielding a nanocrescent with a thickness of ~100 nm. A fillet with a radius of curvature of 1 nm was used on the tip of the nanocrescent to better represent the fabricated structure. Adaptive meshing was employed to automatically reduce the mesh element size near geometric edges that were rapidly changing within the structure until the maximum field converged. A 200 nm-diameter pillar with a height of 200 nm was added below the planar nanocrescent. The 2-D composite structure was then revolved 360° around the *z*-axis to form the 3-D nanotorch structure with a rim opening of 140 nm.

The plasmon resonance can also be tuned by varying the cavity offset of the inner dielectric sphere (*i.e.*, air in the simulation). Changing the offset will invariably affect the rim diameter and the thickness. In planar 2-D nanocrescent structures, this translates to tip-to-tip distance and as the offset decreases, the dipole-like coupling increases between the tip, resulting in increased resonance as demonstrated experimentally.[3,5] For our 3-D nanotorch simulations, the offset and thickness were kept constant. To introduce larger rim opening, the planar nanocrescent was truncated before the 360° revolution in the model. The same 150 nm and 200 nm radii circles were used with the same offset. The planar structure was truncated to create an opening of 130 nm (in radius) and then a 1 nm fillet was performed at the tip. After 360° revolution, a 3-D nanotorch with a rim opening of 260 nm was simulated using adaptive meshing. In the first case of a nanotorch with a rim opening of 140 nm (as shown in Fig. 1a), a maximum electric field of 45 V m^{-1} at the rim was achieved with ~400 K meshing elements. This is in contrast to a lower value of 29.7 V m^{-1} for the 260 nm rim opening case with ~610 K meshing elements (as shown in Fig. 1b). The 260 nm opening has a smaller amplitude compared to the 140 nm opening due to less plasmonic coupling between the cavity and the edges. We have also investigated different nanotorch sizes and found that the resonance peak is red-shifted as the size increases and the resonance is broadened, which is consistent with the size-effect seen in gold nanoparticles.[12] We found in the simulations that the nanotorch and the nanocrescent behave similarly in terms of the location and the magnitude of the maximum electric field being concentrated on the rim of the structure. The maximum near-field increases significantly as the fillet radius decreases, especially below 1 nm. Increasing the sharpness of the tip (rim) will increase the lightning rod effect but has little effect on the dipole-like coupling between the tips and cavity. For a fillet radius of 0.25 nm and a correspondingly smaller rim diameter of 72 nm, the total adaptive meshing element count is ~770 K elements with a maximum electric field of 190 V m^{-1}. However, a fillet of 1 nm was chosen in our simulations to better represent actual fabricated structures instead of trying to report the highest maximum field with the unrealistic 0.25 nm fillet for fabricated structures.

2.2 Fabrication method

Lu *et al.* had previously fabricated nanocrescents with the substrate placed above the sputtering cathode at a tilt angle of ~30° as the substrate was rotated.[2] Here, we analyse two sputtering setups for our sputtering machine. The first is analogous to their setup except that the substrate was placed on a horizontal rotating stage below the sputtering cathode at an angle of $\theta \sim 30°$, as shown in Fig. 2a. The opening of the nanocrescent is calculated to be $d = r(\sin \beta)$, Fig. 2b, where for a 150 nm-radius nanoparticle and β of 60° , the rim opening is $2d = 260$ nm. In this setup, as well as in ref. 2, the nanoparticles rest on top of a horizontal planar surface and because of the shadowing effect of the sputtering cathode onto the nanoparticles, it is impossible to fabricate nanocrescents with a small rim opening.

The second fabrication setup is shown in Fig. 2c with the nanoparticles resting on nanopillars. The substrate is secured on a custom-made, rotating plate mounted onto a motor that is

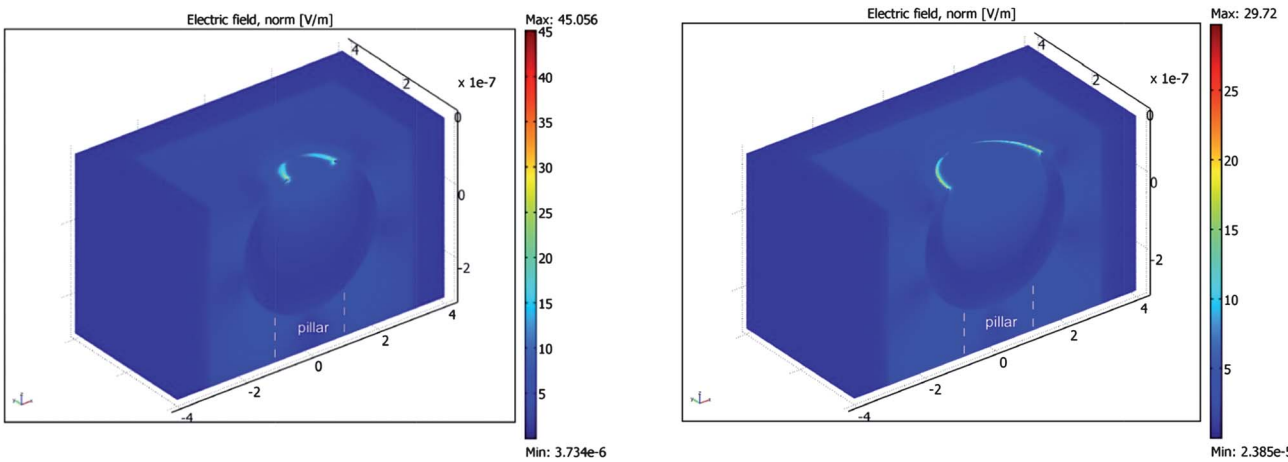

Fig. 1 3-D FEM simulation of the nanotorch structure comprising of a 100 nm-thick gold nanocrescent on top of a 200 nm pillar. A fillet with a 1 nm radius was applied to the tip. Only half of the structure is shown to better reveal its cross-section. (a) The rim opening is 140 nm. (b) The rim opening is 260 nm.

Downloaded by University of California - San Diego on 03 December 2012
Published on 14 September 2012 on http://pubs.rsc.org | doi:10.1039/C2NR32305B

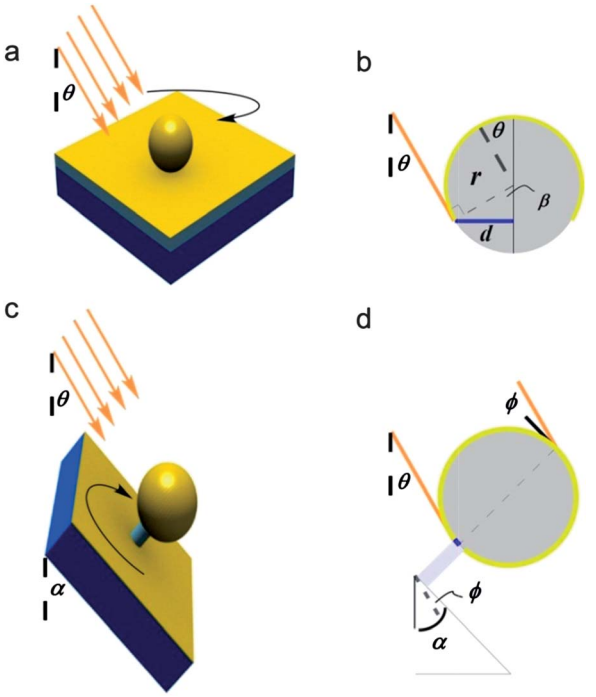

Fig. 2 (a) Metal deposition setup for nanocrescents with large rim opening. (b) Geometrical schematic of the traditional fabrication method with the opening given by length $2d$. (c) Metal deposition setup with a nanoparticle sitting on a nanopillar mounted on a goniometer for fabricating nanotorch structure with controllable rim opening and deterministic orientation. (d) Geometric schematic of the proposed deposition process where the opening is determined by the diameter of the nanopillar.

secured onto a goniometer to control the relative angle of incidence between the sputtering cathode and the rotating stage. In the proposed setup, the goniometer is set to 45° so the entire surface area of the nanoparticles is coated with metal except for the small portion that is in contact with the nanopillars. The rim opening is dependent on the diameter of the nanopillar under the condition that the angle α is larger than θ, Fig. 2d. By changing the goniometer angle, α, the ϕ angle is altered, which will affect the shape of the nanostructure. For $\phi = 0$, we could get nanoring-like structures, similar to ref. 13.

Silica nanoparticles were used as sacrificial templates for fabricating these upright nanotorches. The nanoparticle solution was diluted to ensure an isolated nanoparticle in order to analyse the SERS effect on an individual nanotorch. Subsequently, a poly-(methyl methacrylate) (PMMA) photoresist was spun onto a cleaned microscope slide substrate (or silicon substrate) and baked. The sample was then dipped vertically into the silica nanoparticle solution and then brought up slowly. As water molecules evaporated from the surface, randomly distributed and isolated nanoparticles were dispersed onto the substrate (Fig. 3a). It was found experimentally that this technique provided much better dispersion than the spin coating technique. The samples were then mounted onto a custom-made rotating stage which was secured onto a goniometer stage as discussed previously. Reactive ion etching (RIE) was then used to create nanopillars in which the silica nanoparticles act as the etching

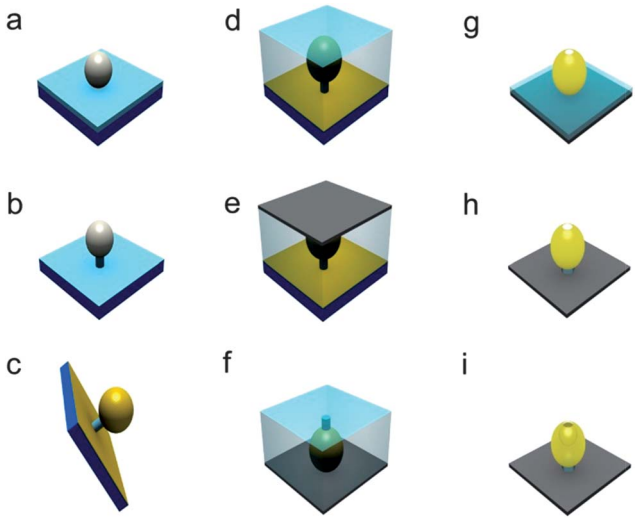

Fig. 3 Fabrication process. (a) Silica nanoparticle on a photoresist-coated BK7 substrate. (b) RIE etching to create nanopillar in order to fabricate nanotorch with small rim opening. (c) Oblique metal sputtering using setup in Fig. 2c. (d) Embedding nanoparticle with ETPTA monomer. (e) Binding to silicon wafer. (f) After peeling and transferring to silicon wafer. (g) RIE etching of ETPTA down to nanoparticle to create nanocrescent. (h) Further RIE etching to create nanotorch structure. (i) Dissolve sacrificial, silica nanoparticle to create nanotorch.

mask, as shown in Fig. 3b and 4a of a scanning electron microscopy (SEM) image. The girth of the nanopillar can be adjusted by varying the etching condition. Nanopillars as small as 50 nm-diameter have been demonstrated. The nanopillar will subsequently dictate the opening of the nanotorch together with the sputtering setup. An adhesion layer of chromium (~1 nm)

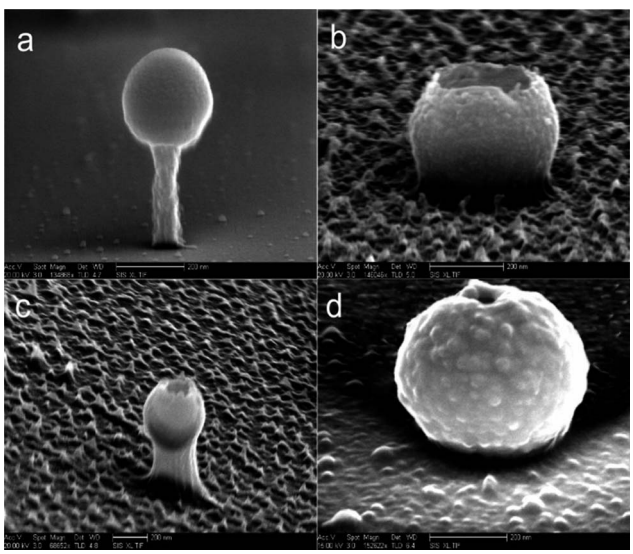

Fig. 4 (a) After RIE etching of PMMA to create nanopillar where the silica nanoparticle acts as etching mask. (b) Upright nanocrescent structure with larger rim opening (~260 nm) fabricated with the setup shown in Fig. 2a. (c) Upright nanotorch structure with smaller rim opening (~140 nm) fabricated using the goniometer setup shown in Fig. 2c. (d) Even smaller rim opening (~50 nm) has been demonstrated.

This journal is © The Royal Society of Chemistry 2012

Published on 14 September 2012 on http://pubs.rsc.org | doi:10.1039/C2NR32305B
Downloaded by University of California - San Diego on 03 December 2012

was then sputtered onto the nanoparticles with a goniometer angle (α) of 45° . Subsequently, a gold thickness of 100 nm was sputtered, followed by another sputtering step of chromium (~2 nm) to protect the gold material during a later RIE etching process to create the nanotorch pillar (Fig. 3c).

Diluted ethoxylated trimethylolpropane triacrylate (ETPTA) monomer was then mixed with 20% photoinitiator, spun onto the metal-coated silica nanoparticles and slowly ramped up to embed the nanoparticles inside this monomer layer. The sample was then polymerized with a UV light source (Fig. 3d). A clean silicon substrate was then primed with (3-acryloxypropyl) trichlorosilane (APTCS) for adhesion to the nanoparticle-embedded ETPTA sample. The two pieces were bonded and then baked on a hot plate before peeling apart the two pieces (Fig. 3e). After transferring to the silicon substrate, chromium and gold wet etchants were used to remove the metals on the surface of the monomer (Fig. 3f). The metals on the nanoparticles are protected from this wet etching process since they are embedded inside the monomer. The sample was then RIE etched again to remove the ETPTA layer down to the nanoparticle-level to create nanocrescents (Fig. 3g). To create the nanotorches, the etching time was prolonged to form the nanotorches' nanopillars (Fig. 3h). Lastly, the sample was dipped and agitated lightly in a 4% diluted hydrogen fluoride solution to dissolve the silica nanoparticles to produce these nanotorch structures, as shown in Fig. 3i. Before SERS characterization, chromium wet etchant was used again to remove chromium from the nanotorch structure and expose the gold to analyte adsorption. With the sputtering setup shown in Fig. 2a, upright-oriented nanocrescents and nanotorches with large rim opening were fabricated as shown in Fig. 4b with a nanocrescent with an opening of ~260 nm. With the new sputtering setup shown in Fig. 2c and a goniometer angle α of 45°, upright-oriented nanocrescents and nanotorches with a smaller rim opening were fabricated as shown in Fig. 4c with a nanotorch rim opening of ~140 nm. Using this technique, we have demonstrated as small as ~50 nm-diameter rim opening as shown in Fig. 4d.

2.3 SERS enhancement factor and uniformity measurements

For SERS characterization, a near infrared (NIR) 785 nm laser was used not only because it better matched the scattering resonance of the nanotorch but also because it can avoid the fluorescence from biomolecules. It has a deeper penetration depth in biological issues, and the low photon energy minimizes photothermal damage to biomolecules and cells.[2,14] Moreover, by using a NIR source, it ensures that the detected SERS signal is from the nanotorch and not from residual nanoparticles since the plasmon resonance of the nanoparticle can hardly be excited by a NIR source—a necessary condition for the effective near-field energy transfer to adsorbed molecules as manifested by the SERS enhancement phenomenon.[15] Kneipp *et al.* had shown a SERS enhancement factor (EF) of ~10^9 by using an 830 nm laser beam on a cluster of nanoparticles.[16] However, due to the random particle aggregation, locating these hot spots in the interstitial spacing of the nanoparticle cluster is unpredictable and non-uniform. In the case of the nanotorch, the SERS enhancement of each single nanotorch does not depend on the coupling between multiple nanoparticles but rather on the resonant coupling of the sharp tips, inner cavity edges and outer edges, making it an individual single SERS substrate.

The measured Raman spectra are shown in the bottom, middle, and top spectrum in Fig. 5a for the neat benzenethiol (magnified 5 times), the nanotorch with a 260 nm opening, and the nanotorch with a 140 nm opening, respectively. The modes of the spectra correspond to those of published reports of benzenethiol adsorbed onto gold[17] and the monolayer coverage of benzenethiol is confirmed by the absence of the C–S bond in the SERS spectra at around 2561 cm^{-1} (not shown).[18,19] No Raman signal was seen for measurement done on bare silicon sample sputtered with gold under the same sputtering condition. A conservative estimate of the enhancement factor is ~8.2×10^6 for the 140 nm-opening nanotorch, which is ~6× higher than compare to the 260 nm-opening nanotorch with an EF of 1.5×10^6.

More importantly, shown in Fig. 5b is a representative waterfall plot of five Raman measurements of individual nanotorches at different locations within the sample. The standard deviations of the Raman intensity at each mode, shown in Table 1 corresponding to 1000 cm^{-1}, 1023 cm^{-1}, 1074 cm^{-1}, and 1573 cm^{-1} wavenumbers, are all calculated to be less than 20%. We attribute the uniformity of the Raman intensity to the upright orientation of the nanotorches and therefore, the consistent orientation of the incident field relative to the nanotorches

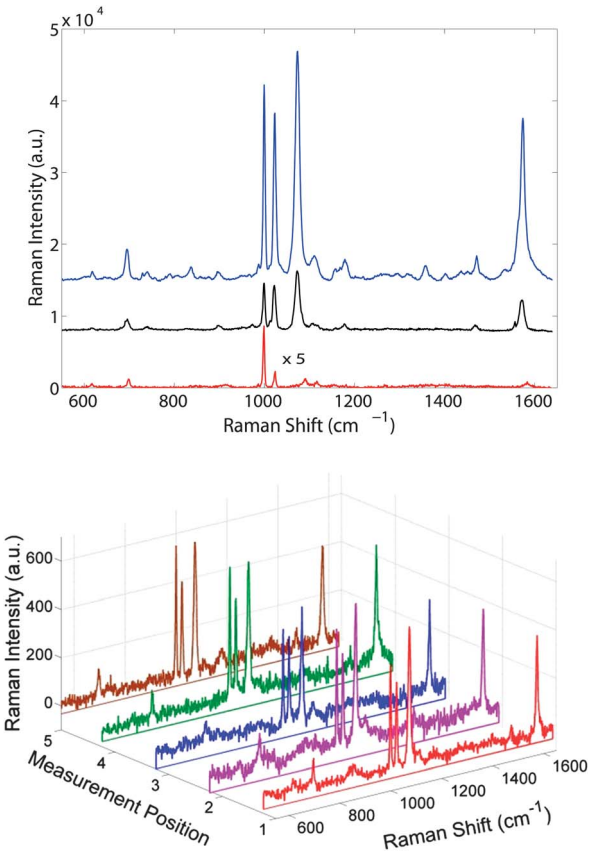

Fig. 5 (a) The measured Raman signals for a 140 nm opening nanotorch (top), a 260 nm opening nanotorch (middle), and neat benzenethiol (bottom). (b) A sample uniformity plot of 5 nanotorches at different locations within the same substrate.

Published on 14 September 2012 on http://pubs.rsc.org | doi:10.1039/C2NR32305B
Downloaded by University of California - San Diego on 03 December 2012

Table 1 The standard deviation of the Raman intensity for benzenethiol adsorbed onto the gold nanotorch

Peak [cm^{-1}]	Mode	Std. dev.
1000	ν(C–C–C)	20.0%
1023	ν(C–H)	12.3%
1074	ν(C–C–C) and ν(C–S)	12.6%
1573	ν(C–C–C)	16.5%

resulting from the new fabrication technique. A previous fabrication method had yielded nanocrescents exhibiting different scattering spectra within the same substrate, in which the authors attributed to slight difference in the geometries and the orientations with respect to the incident light.[2] As a result of their fabrication method, the orientation of the nanocrescents varied. Since the near-field enhancement is largely influenced by the orientation of the incident field, the non-uniformity in their measurements was observed. Using our proposed fabrication method, the upright-oriented nanotorches yielded better than 80% Raman signal uniformity.

2.4 Discussion

It is important to note that the enhancement factor calculation is a conservative estimate since it is assumed that the surface of the nanotorch is saturated with benzenethiol, which is probably not the case in the experiment. In addition, as can be seen from the FEM simulation, only the rim has high electrical field concentration and contributes to the enhancement effect. The percentage of the concentrated electrical field on the rim relative to the total surface area of the nanotorch is 0.8%. The total number of benzenethiol molecules contributing to the enhancement effect is estimated to be ~15 000. Further experiments are on-going to optimize the nanotorch geometry to yield an even higher enhancement factor by changing the gold thickness, the rim opening, and the goniometer angle. We have fabricated 50 nm-diameter rim opening nanotorches, but challenges were encountered in keeping these structures upright consistently during the fabrication process as the nanoparticles tend to fall off the nanopillars during the fabrication process. Dip-coating and vapor deposition will be investigated to solve this issue to create an even smaller rim diameter to achieve an even higher enhancement factor. It is envisioned in the future that these nanotorch structures could be integrated into opto-fluidic chips such that biomolecules could be controlled onto the rims of the nanotorches *via* electrokinetic forces for maximum enhancement efficiency.[20] Furthermore, significant progress has been made in the fabrication of periodic nanoparticle arrays recently.[20–22] By using these and other methods, fabrication of 3-D nanotorch arrays will be investigated to yield an even higher enhancement factor due to the coherent coupling effect of the periodic array. Moreover, nanotorch arrays will increase the spatial resolution of SERS substrate, enabling SERS imaging and *in vivo* diagnosis.

3. Conclusions

Three-dimensional FEM simulations of nanotorch were performed and validated that a smaller cavity rim opening will produce a higher local field enhancement and thus higher SERS enhancement factor due to enhanced plasmonic coupling between the cavity mode and the edges. We introduced a method of fabricating upright nanotorches with controllable cavity opening and deterministic orientation that yielded uniform Raman intensity of better than 80%. Each nanotorch serves as a single SERS substrate. Measurements confirmed that a smaller rim opening (140 nm diameter) yielded an enhancement factor approximately 6 times higher than a larger rim opening (260 nm diameter). The higher enhancement factor of the fabricated 3-D nanotorch can be used for *in vivo* diagnosis to replace nanoparticle clusters for better limit of detection.

4. Experimental section

4.1 Nanosphere template fabrication

Specifically, 310 nm silica nanoparticles (from Bangs Laboratory) were made into 0.002% solution in 18 MOhm purified water (from ThermoScientific Barnstead Nanopure System) with 0.001% of surfactant (Tween 20, from SigmaAlrich) to prevent coagulation. BK7 microscope slides were diced, cleaned with piranha solution and DI water, and then dried with nitrogen. Subsequently, poly-(methyl methacrylate) (PMMA) A4 (from MicroChem) was spun at 4000 rpm for 45 s onto the sample substrate and baked for 1 min at 180 °C on a hotplate. The sample was then dipped vertically into the silica nanoparticle solution for 30 s and then brought up slowly. Reactive ion etching (RIE) was then used to create nanopillars in which the silica nanoparticles act as an etching mask. The girth of the nanopillar pedestal can be controlled by adjusting the etching condition. We have demonstrated as small as 50 nm-diameter pedestal using the Oxford PlasmaLab 80 RIE machine. RF Metal sputtering was performed using Denton Discovery 18. Diluted ethoxylated trimethylol propane triacrylate (ETPTA) monomer (SR415, Sartomer Inc.) was mixed with 20% (2-hydroxy-2-methyl-1-phenyl-1-propanone) photoinitiator (Darocur 1173, BASF Corp.). The samples were then polymerized with the UV light source of a mask aligner (MA6, Karl Suss). A clean silicon wafer was then primed with (3-acryloxypropyl) trichlorosilane (APTCS) (Gelest Corp.) and rinsed with ethanol. The silicon wafer was next bonded to the nanoparticle-embedded ETPTA sample. They were baked on a hot plate at 60 °C for 30 min before peeling apart the two pieces. The ETPTA layer was etched using the PlasmaLab80 machine at 100 W with 40 sccm of O_2, 40 mTorr for 90 s. To create the nanotorch, the etching time was prolonged to 3 min. Lastly, the sample was dipped and lightly agitated with a pair of tweezers in a 4% diluted HF solution to dissolve the silica nanoparticles for 3 min to produce the nanotorches. The substrates were treated with 5 mM of benzenethiol in 200-proof bioagent grade ethanol (from SigmaAlrich) for 3 hours and then rinsed copiously with ethanol 3 times and then carefully dried with nitrogen.

4.2 SERS measurement

Raman measurements were taken using the inVia Raman microscope system from Renishaw Inc. with a 785 nm excitation

 This journal is © The Royal Society of Chemistry 2012

source. The substrates were immersed in the benzenethiol analyte and then rinsed and dried. At first, a coarse Raman image mapping was done on the sample using the built-in Raman imaging feature to ensure that we were looking at the nanotorch structure. The distance between nanotorches is greater than 3 μm and the average density is approximately one nanotorch per 10 μm^2 area. Next, a 50× objective was positioned over the hot spot seen on the image mapping and several static measurements were taken on and around the hot spot by moving the position of the substrate incrementally to maximize the Raman signal to ensure that the laser beam is focused on the nanotorch. If only one monolayer of benzenethiol exists on a flat gold surface, the surface coverage is equivalent to 0.6 nmol cm^{-2}.[23] We have considered the Raman intensities of the 1573 cm^{-1} band (C–C stretching mode) to calculate the approximate enhancement factor because of its appearance in both the neat and SERS spectra. It should be noted that for the neat spectrum, there is a slight shift for the neat Raman measurement to 1584 cm^{-1}. The surface area of the nanotorch (100 nm-thick nanocrescent fabricated from the 310 nm silica nanoparticle) with benzenethiol adsorbed onto gold is approximately that of an equivalent nanoparticle with a diameter of 410 nm. Assuming a decay length of 20 nm, the 140 nm rim diameter has an effective area of (pi $[r_{outer}^2 - r_{inner}^2] = 4.4 \times 10^{-11}$ cm^2). The total number of benzenethiol molecules contributing to the enhancement effect is estimated to be ~15 000 (4.4×10^{-11} $cm^2 \times 0.6$ nmol $cm^{-2} \times 6.02 \times 10^{23}$).

Acknowledgements

The authors thank L. Cambrea of NAWCWD for initial discussion on SERS detection. This work was funded by the DARPA Center for Opto-Fluidic Integration, NSF, NSF's CIAN ERC, and Cymer Corporation.

Notes and references

1 D. P. Fromm, A. Sundaramurthy, A. Kinkhabwala, P. J. Schuck, G. S. Kino and W. E. Moerner, *J. Chem. Phys.*, 2006, **124**, 061101.
2 Y. Lu, G. L. Liu, J. Kim, Y. X. Mejia and L. P. Lee, *Nano Lett.*, 2005, **5**, 119.
3 H. Rochholz, N. Bocchio and M. Kreiter, *New J. Phys.*, 2007, **9**, 53.
4 J. S. Shumaker-Parry, H. Rochholz and M. Kreiter, *Adv. Mater.*, 2005, **17**, 2131.
5 K. Li, L. Clime, B. Cui and T. Veres, *Nanotechnology*, 2008, **19**, 145305.
6 R. Bukasov and J. S. Shumaker-Parry, *Nano Lett.*, 2007, **7**, 1113.
7 X. Liu, N. C. Linn, C.-H. Sun and P. Jiang, *Phys. Chem. Chem. Phys.*, 2010, **12**, 1379.
8 J. Kim, G. L. Liu, Y. Lu and L. P. Lee, *Opt. Express*, 2005, **13**, 8332.
9 B. M. Ross and L. P. Lee, *Nanotechnology*, 2008, **19**, 275201.
10 F. Hao, P. Nordlander, Y. Sonnefraud, P. V. Dorpe and S. A. Maier, *ACS Nano*, 2009, **3**, 643.
11 Y. Zhang, T. Q. Jia, D. H. Feng and Z. Z. Xu, *Appl. Phys. Lett.*, 2011, **98**, 163110.
12 S. Link and M. A. El-Sayed, *J. Phys. Chem. B*, 1999, **103**, 8410.
13 J. Aizpurua, P. Hanarp, D. Sutherland, M. Käll, G. Bryant and F. García de Abajo, *Phys. Rev. Lett.*, 2003, **90**, 57401.
14 K. Kneipp, A. S. Haka, H. Kneipp, K. Badizadegan, N. Yoshizawa, C. Boone, K. E. Shafer-Peltier, J. T. Motz, R. R. Dasari and M. S. Feld, *Appl. Spectrosc.*, 2002, **56**, 150.
15 A. M. Michaels, M. Nirmal and L. E. Brus, *J. Am. Chem. Soc.*, 1999, **121**, 9932.
16 K. Kneipp, H. Kneipp, R. Manoharan, E. B. Hanlon, I. Itzkan, R. R. Dasari and M. S. Feld, *Appl. Spectrosc.*, 1998, **52**, 1493.
17 R. L. Aggarwal, L. W. Farrar, E. D. Diebold and D. L. Polla, *J. Raman Spectrosc.*, 2009, **40**, 1331.
18 C. A. Szafranski, W. Tanner, P. E. Laibinis and R. L. Garrell, *Langmuir*, 1998, **14**, 3570.
19 S. W. Han, S. J. Lee and K. Kim, *Langmuir*, 2001, **17**, 6981.
20 H. M. Chen, L. Pang, M. S. Gordon and Y. Fainman, *Small*, 2011, **7**, 2750.
21 Y. Xia, Y. Yin, Y. Lu and J. McLellan, *Adv. Funct. Mater.*, 2003, **13**, 907.
22 Y. Cui, M. T. Björk, J. A. Liddle, C. Sönnichsen, B. Boussert and A. P. Alivisatos, *Nano Lett.*, 2004, **4**, 1093.
23 L.-J. Wan, M. Terashima, H. Noda and M. Osawa, *J. Phys. Chem. B*, 2000, **104**, 3563.

Published on 14 September 2012 on http://pubs.rsc.org | doi:10.1039/C2NR32305B
Downloaded by University of California - San Diego on 03 December 2012